Supporting Information

for

ELDOR-detected NMR (EDNMR) to Measure Metal Hyperfine Interactions: ^{61}Ni in the Ni-B state of the [NiFe] Hydrogenase of *Desulfovibrio vulgaris* Miyazaki F

Marco Flores, Aruna Goenka Agrawal, Maurice van Gastel, Wolfgang Gärtner, Wolfgang Lubitz*

Max-Planck-Institute for Bioinorganic Chemistry, Stiftstrasse 34-36, D-45470 Mülheim an der Ruhr, Germany

Spin Hamiltonian. The observed ^{61}Ni ELDOR-detected NMR spectra were interpreted using a spin Hamiltonian, $\mathcal{H}$, containing the electron and nuclear Zeeman interactions with the applied magnetic field $\mathbf{B_o}$, the hyperfine coupling (hfc) and the nuclear quadrupole coupling (nqc) terms:

$$\mathcal{H} = \beta_e\, \mathbf{S}\cdot\boldsymbol{g}\cdot\mathbf{B_o} - \beta_N\, g_N\, \mathbf{I}\cdot\mathbf{B_o} + h\, \mathbf{S}\cdot\boldsymbol{A}\cdot\mathbf{I} + h\, \mathbf{I}\cdot\boldsymbol{P}\cdot\mathbf{I} \quad (1),$$

where **S** is the electron spin operator, **I** is the nuclear spin operator of ^{61}Ni; $\boldsymbol{A}$ and $\boldsymbol{P}$ are the hfc and nqc tensors in frequency units, $\boldsymbol{g}$ is the electronic g–tensor, h is Planck's constant, g_N is the g–factor of the corresponding magnetic nucleus (^{61}Ni) and β_e and β_N are the electron and nuclear magnetons, respectively. Thus, the energy of the spin system (S = ½, I = 3/2) is obtained to first order for a given direction of the magnetic field by:

$$E_{M_S,M_I} = g\beta_e B_o M_S - g_N\beta_N B_o M_I + A\, h\, M_S M_I + \frac{3}{2}\, P\, h\, [\, M_I^2 - \frac{1}{3} I\,(I+1)] \quad (2),$$

where M_S is the magnetic quantum number of the electron (±½), M_I the magnetic quantum number of the nucleus (±3/2, ±½), A and P are the hfc and nqc along the magnetic field direction, respectively.

Definition of Transitions. Three types of transitions can be defined following the respective selection rules:

i) NMR transitions, i.e. $\Delta M_S = 0$, $\Delta M_I = \pm 1$ (driven in ENDOR experiments):

$$\nu^{ENDOR} = (\, E_{M_S,M_I} - E_{M_S,M_I \pm 1}\,)/h \quad (3).$$

ii) EPR forbidden transitions, i.e. $\Delta M_S = \pm 1$, $\Delta M_I \neq 0$ (driven in EDNMR experiments using ν_1). For ^{61}Ni, $\Delta M_I = \pm 1, \pm 2, \pm 3$. When $\Delta M_I = \pm 1$, the resonance frequency ν_1 is given by:

$$\nu_1 = (\, E_{M_S,M_I} - E_{M_S \pm 1,M_I \pm 1}\,)/h \quad (4).$$

iii) EPR allowed transitions, i.e. $\Delta M_S = \pm 1$, $\Delta M_I = 0$ (driven while detecting using ν_2):

$$\nu_2 = (\, E_{M_S,M_I} - E_{M_S \pm 1,M_I}\,)/h \quad (5).$$

In EDNMR experiments, the changes in the EPR signal are detected with respect to the shift between the two MW frequencies ($\nu_1 - \nu_2$). Therefore, the EDNMR resonances for $\Delta M_S = \pm 1$ and $\Delta M_I = \pm 1$ are:

$$\nu_1 - \nu_2 = (\, E_{M_S \pm 1,M_I} - E_{M_S \pm 1,M_I \pm 1}\,)/h \quad (6),$$

as obtained using Eqs. (4) and (5). Since Eq. (6) is independent of $M_S \pm 1$ for S = ½ systems, it can be rewritten as:

$$\nu_1 - \nu_2 = (\, E_{M_S,M_I} - E_{M_S,M_I \pm 1}\,)/h \quad (7).$$

Eq. (7) gives the same resonances obtained for the ENDOR experiment (see Eq. (3)). Using Eq. (2), it can be written as:

$$|\, \nu_1 - \nu_2 \,| = |\, + A\, M_S - g_N\beta_N B_o/h + \frac{3}{2}\, P\, (2\, M_I - 1)\,| \quad (8).$$

For a system with a dominant hfc interaction (i.e. $A/2 >> g_N\beta_N B_o/h$), the EDNMR resonances ($\Delta M_S = \pm 1$ and $\Delta M_I = \pm 1$) occur around $A/2$ (see Fig. S1). Consistently, the EDNMR resonances corresponding to $\Delta M_I = \pm 2$ and $\Delta M_I = \pm 3$ occur around A and $3A/2$, respectively.

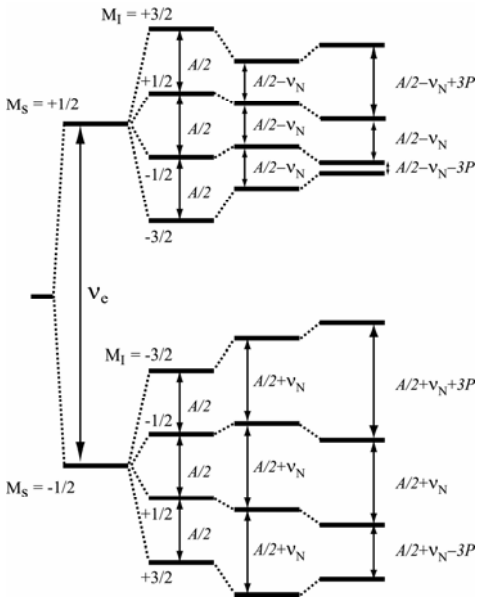

Figure S1. Energy scheme for a spin system, S = ½ and I = 3/2, with a dominant hfc interaction. The arrows on the further right indicate the NMR transitions (frequencies) that would be observed in the ENDOR experiment ($\nu_e = g\beta_e B_o/h$, $\nu_N = g_N\beta_N B_o/h$). These frequencies were used to simulate the EDNMR signals around $A/2$.

Fit of CW EPR Spectra. The principal components of the ^{61}Ni hfc tensor corresponding to Ni-B were obtained from EPR by simulating the difference in linewidth of cw EPR spectra of $^{58/60}$Ni (I = 0) and ^{61}Ni (I = 3/2) enriched samples (see Fig. S2). The simulations were performed using the spin Hamiltonian described above (see Eq. (1)). The fitting procedure was similar to that described in ref. 17.

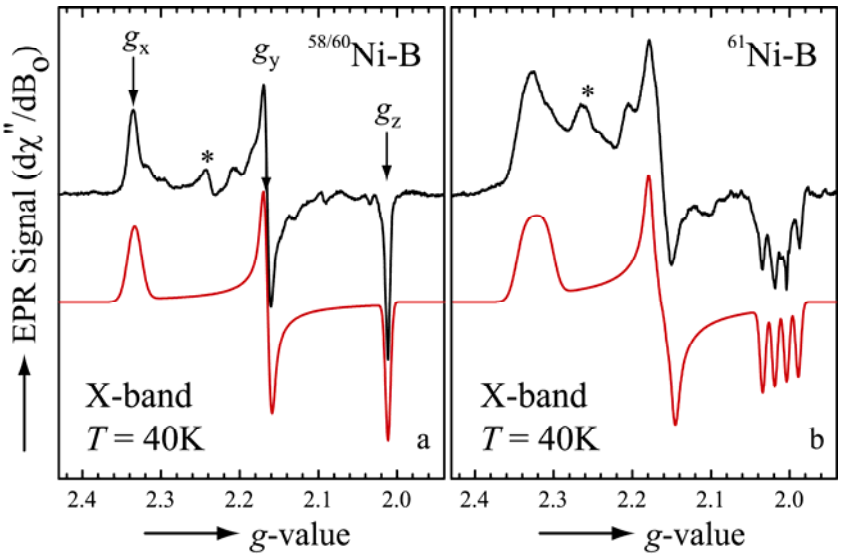

Figure S2. Experimental (black) and simulated (red) cw EPR spectra of Ni-B corresponding to $^{58/60}$Ni and ^{61}Ni samples. These spectra contain additional small signals (contaminations), which include 10%-20% of Ni-A (marked with *). The spectrum of ^{61}Ni-B clearly shows the effect of the isotope labeling. The $^{58/60}$Ni-B spectrum was fitted using the principal components of the g–tensor (g_x, g_y, g_z) and the line-widths (ΔB_x, ΔB_y, ΔB_z) as fitting parameters (see Table S2.1). The ^{61}Ni-B spectrum was fitted by optimizing the principal components of the hfc tensor ($A_{x'}$, $A_{y'}$, $A_{z'}$) and the Euler angles (ϕ, θ, ψ) that describe its orientation with respect to the principal axes x, y, z of the g-tensor of Ni-B (see Table S2.2), whereas g_x, g_y, g_z, ΔB_x, ΔB_y and ΔB_z were fixed at the values (see Table S2.1) obtained from the fitting of the spectrum corresponding to the non-enriched sample.

Table S2.1. g–values and linewidths obtained by fitting the EPR spectrum of the $^{58/60}$Ni-B sample.

	g_x [±0.005]	g_y [±0.005]	g_z [±0.005]	ΔB_x [MHz]	ΔB_y [MHz]	ΔB_z [MHz]
EPR	2.334	2.163	2.010	86	44	37

Fit of EDNMR Spectra. These spectra were fitted considering the following parameters: Principal components of the hfc tensor, Euler angles relating hfc and **g** tensors (see ref. 2 for Euler angles definition), and the EDNMR linewidths ($\Delta\nu_k$, with k = 1,…, 7). This was performed using a routine written in Matlab (The MathWorks, Natick, MA).

Table S2.2. Principal components and Euler angles of the ^{61}Ni hfc tensor obtained by fitting EPR (see Fig. S2) and EDNMR (see Fig. 2) spectra. Although, the EDNMR spectra contain signals corresponding to nuclear magnetic transitions around $\pm A/2$, $\pm A$ and $\pm 3A/2$ (see Fig. 2b), only the signals around $\pm A/2$ were simulated (see Fig. 2c). The intensities of the signals around $+A/2$ are slightly different than those of the signals around $-A/2$. The simulated spectra were scaled to the intensity of the experimental spectra. The magnitudes and orientation of the ^{61}Ni hfc tensor obtained from EDNMR are more accurate than those obtained from EPR. For the definition of Euler angles see ref. 2. From the 8 possible solutions we picked the one most compatible with the X-ray structure (ref. 7).

	$A_{x'}$ [MHz]	$A_{y'}$ [MHz]	$A_{z'}$ [MHz]	ϕ [deg]	θ [deg]	ψ [deg]
EPR	-47 ± 10	-36 ± 3	-71 ± 5	-5 ± 30	10 ± 25	15 ± 33
EDNMR	-41 ± 1	-38 ± 1	-71 ± 1	-4 ± 2	-4 ± 1	-13 ± 3

Table S2.3. EDNMR linewidths ($\Delta\nu_k$) obtained from the fit of the EDNMR spectra (see Fig. 2). The EDNMR linewidth was modeled using a different linewidth parameter for each EDNMR spectrum (B_1,…,B_7). The nqc is not resolved in the spectra ($6P$ in the case of ^{61}Ni, see Fig. S1), however an upper limit can be estimated from the largest EDNMR linewidth ($\Delta\nu_7$). Thus, the largest splitting is smaller than the largest linewidth, i.e., $6P_z < 15$ MHz.

	$\Delta\nu_1$ [MHz]	$\Delta\nu_2$ [MHz]	$\Delta\nu_3$ [MHz]	$\Delta\nu_4$ [MHz]	$\Delta\nu_5$ [MHz]	$\Delta\nu_6$ [MHz]	$\Delta\nu_7$ [MHz]
EDNMR	10.1	10.4	8.9	8.9	11.6	15.0	15.1